Amyloids: from molecular structure to mechanical properties

Gelderloos, C.C.

2014

document version
Publisher's PDF, also known as Version of record

Chapter 7

Measuring the bending rigidity of amyloid fibrils in solution

Based on: Corianne C. van den Akker, Floortje P. van de Poll, Paul J. Atzberger, Gijsje H. Koenderink (submission in preparation).

Abstract

Amyloid fibrils are fibrillar protein aggregates formed from (partly) unfolded proteins or peptides. They possess a high mechanical stiffness and strength, making them interesting candidates for applications in materials science or food texturing. A common measure of the mechanical properties of semiflexible fibers such as amyloids is the persistence length, L_p, which characterizes the bending rigidity. L_p has been determined for a variety of amyloid fibrils based on electron microscopy or atomic force microscopy imaging of an ensemble of fibrils immobilized on a flat support. However, deposition and drying of protein fibrils on a surface can potentially affect their conformation and structure. Furthermore, because measurements are averaged over a large number of fibrils, it is not possible to identify the polymorphism of amyloid fibrils. Here we determined the persistence length of amyloid fibrils formed from hen egg white lysozyme (HEWL) using two different approaches. The first approach was the standard atomic force microscopy approach, which involves imaging of a large ensemble of fibrils combined with image analysis to obtain the fiber conformations. We observed an average persistence length ranging between 2.5 and 4.4 μm, depending on the surface (mica or glass) on which the fibrils were immobilized and on fibril hydration. The second approach was to obtain time-lapse movies by fluorescence microscopy of the thermal bending undulations of freely fluctuating fibrils suspended in water. We observed a strikingly large variation in the persistence length of individual fibrils. For 8 fibrils, the persistence length varied between 0.7 to 6.7 μm, and for 2 fibrils the persistence length was even too large to measure by video microscopy. In summary, the two different techniques give similar average values of L_p in the range of several micrometers, but time-lapse imaging reveals a large variability for fibrils within the same sample. This variability is a signature of the structural polymorphism of amyloid fibrils.

Introduction

Amyloid fibrils are a broad class of biopolymers that can form by self-assembly from peptides or proteins that are in an unfolded or misfolded state.[1] It is thought that almost every (poly)peptide will form amyloids under appropriate conditions.[1] Some amyloids are associated with diseases like Alzheimer's disease and type II diabetes mellitus[2], where oligomers or fibrils are thought to damage the plasma membrane of cells, thus causing cell death.[3,4] The large mechanical stiffness of amyloid fibrils may contribute to their cytotoxicity.[4,5] Biophysical experiments have shown that amyloid fibrils behave as micron-sized semiflexible polymers with a persistence length that is comparable to their contour length.[6,7] Interestingly, Nature also makes functional use of this stiffness, using benign amyloid fibrils as a structural material for bacterial biofilms and protective shells of certain insect eggs.[8,9] Amyloid fibrils have excellent mechanical properties when compared to other biological and synthetic materials: their Young's modulus is comparable to that of silk and their ultimate tensile strength is comparable to that of steel.[6] Theoretical modeling suggests that these extraordinary mechanical properties mainly derive from the strongly hydrogen-bonded cross-β sheet structure that extends along the backbone of the fibrils.[7] The outstanding mechanical performance of amyloid fibrils coupled with the fact that amyloids can be formed from a wide range of peptide sequences implies that they can be useful for diverse applications. Fibrils formed from food-related proteins are for instance relevant for food texturing.[10] Furthermore, applications in nanostructured materials such as metalized nanowires and in tissue engineering have been suggested.[11-15]

Until now, the stiffness of amyloid fibrils has been investigated mainly by analysis of the conformation of an ensemble of fibrils deposited on a surface and imaged by atomic force microscopy (AFM) or (cryo-)electron microscopy (EM).[16-19] Assuming that the fibrils can be modeled as semiflexible polymers, the bending rigidity can be inferred from the persistence length L_p, which itself follows from the relation between the contour length C and the end-to-end distance E of the fibrils or from the tangent-tangent correlation function. This AFM/EM-based approach provides a global measure of the persistence length of a fibril, because the effect of thermal fluctuations on the chain conformation is evaluated on a large length scale. The AFM/EM-imaging based approach has two important drawbacks. First, the conformation of fibrils adsorbed on a surface is dependent on the strength of the interaction of the fibrils with the surface, as demonstrated by Brownian dynamics simulations and experiments on intermediate filaments and DNA chains adsorbed on different surfaces.[20,21] Second, the fibrils are often dried before imaging, which may affect the morphology and internal structure of the fibrils and thereby their stiffness. A further complicating factor is the well-known

polymorphism of amyloid fibrils, both in length, diameter and internal molecular packing structure.[22] This factor makes it difficult to interpret an average stiffness value based on AFM or EM measurements on an ensemble, and also complicates the interpretation of stiffness measurements obtained by bulk solution techniques such as light or X-ray scattering[23] and rheology[24].

One way to overcome this problem is to actively bend single amyloid fibrils that are deposited across nanoscale grooves using an AFM tip, an approach that has been demonstrated with insulin amyloid fibrils.[6,7] Based on the measured force-distance curves, the bending rigidity and maximal force before breakage could be calculated. An advantage of this technique is that the fibrils are measured in their natural, hydrated state. However, the experiments are technically challenging because of the small diameter of the fibrils.[25] A technically less demanding method to obtain the bending rigidity of fibrils in suspension is to take time-lapse movies of freely fluctuating fibrils in solution by fluorescence microscopy. Rather than extracting the persistence length from the static shapes of an ensemble of fibrils, the persistence length is determined for a single fibril by tracking its shape fluctuations over time. To our knowledge, there is one study where this method was used for amyloid fibrils.[26] The method revealed average persistence lengths of 3.6 and 7.0 μm for two different types of yeast prion amyloid fibrils with contour lengths between 3 and 10 μm and a diameter of 4.5 nm. Force-extension experiments with optical tweezers reported in the same study revealed average persistence lengths of 1.5 and 3.3 μm, respectively. It is possible that the discrepancy is related to structural polymorphism, which is common for amyloid fibrils and should lead to variability in persistence lengths. In addition to the bending rigidity, time-lapse imaging of thermally fluctuating filaments can also reveal the bending dynamics, as demonstrated for actin filaments and microtubules[27-31], as well as carbon nanotubes[32] and DNA nanotubes[33].

Here we investigate the bending rigidity of single amyloid fibrils formed from the model protein hen egg white lysozyme (HEWL), comparing the time-lapse imaging approach where shape fluctuations of single fibrils in solution are analyzed with the more well-established AFM approach of analyzing the shapes of an ensemble of fibrils immobilized on a flat substrate. We perform AFM imaging on dried as well as hydrated fibrils, and compare measurements obtained on two different surfaces, mica and glass. With all analysis methods, we find persistence lengths in the micrometer range. However, the time-lapse imaging approach reveals a remarkable variability of the persistence length among different fibrils, ranging from 0.7 and 6.7 μm for a collection of 8 representative fibrils. This large variability indicates structural polymorphism of fibrils formed under the same conditions.

Results and discussion

To investigate the morphology of the HEWL amyloid fibrils, we performed AFM imaging of fibrils deposited on mica and dried in air. Figure 7.1a shows an AFM image of fibrils formed from HEWL incubated at pH=2.0 and 65°C. The contour length distribution is broad with an average value of 2.6 ± 2.0 µm based on measurement of 275 fibrils (Figure 7.1b). The distribution of the fibril diameters, obtained from the fibril heights, is plotted in Figure 7.1c, showing two distinct populations: one centered around 3.5 nm and another centered around 6 nm. The average diameter was 3.6 ± 1.2 nm, based on diameter measurements on 189 fibrils. The fibrils with diameters around 6 nm are twisted and show a periodicity of approximately 90 nm. These results show that the amyloid sample is polymorphic both in length and diameter. To investigate whether drying affects the fibril morphology, we also imaged hydrated fibrils using liquid AFM. The average diameter was similar to that of the dried fibrils, 3.4 ± 1.1 nm, based on measurements on 128 fibrils, suggesting that drying does not significantly change the morphology. The average length was 1.9 ± 1.3 µm, slightly shorter than that observed for dried fibrils. This difference may be due to a different population of fibrils that binds to the surface for liquid AFM. For liquid AFM, the fibril suspension is 10 times more concentrated compared to the experiments in air, and the binding of fibrils to the surface takes place over hours instead of minutes. The samples for AFM in air are prepared by incubation of a fibril suspension on mica for 3 min and subsequent washing and drying of the sample. Some of the amyloid fibrils are probably washed off the surface. Furthermore, the differences in sample preparation likely affect the equilibration of the fibrils that are bound to the surface. We conclude that drying does not noticeable change the fibril morphology.

We calculated the persistence length as a measure of the bending rigidity of the fibrils based on AFM images of a large ensemble of fibrils. We assume that the fibril conformations are equilibrated before the fibrils adsorb to the surface. This assumption is qualitatively validated by the absence of looped conformations. The energy necessary for creating a bend with an angle Θ in a semi-flexible fibril with a contour length C, Young's modulus Y and area moment of inertia I is given by[21]:

$$E = Y\, I\, \Theta^2 / 2C\ . \qquad (1)$$

According to the equipartition theorem, the persistence length L_p of a thermally fluctuating semiflexible fibril is[21]:

$$Y\, I = k_B\, T\, L_p \qquad (2)$$

where k_B is the Boltzmann constant and T is the temperature.

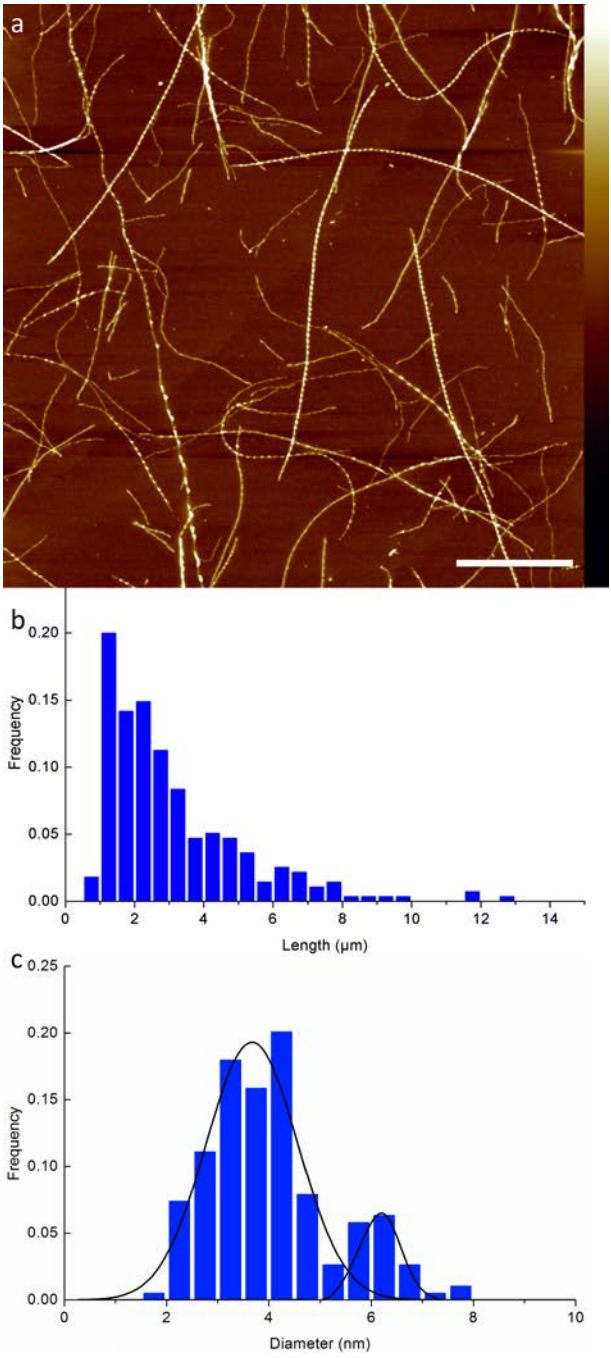

Figure 7.1: a) AFM image of dried HEWL amyloid fibrils at pH=2.0 on mica. Scale bar is 2 µm and height bar is 10 nm. b) Length distribution of 275 HEWL amyloid fibrils measured in AFM images.

c) Diameter distribution of 189 HEWL amyloid fibrils. The distribution is fitted with two Gaussian peaks (black lines).

The normalized probability distribution function in two dimensions for a semiflexible fibril bent by an angle Θ is Gaussian and can be written as[21]:

$$P(\Theta(C))_{2D} = \sqrt{\frac{L_p}{2\pi C}} e^{-L_p\Theta^2/2C} \quad (3)$$

Two different approaches are generally used to infer the average persistence length of the fibrils from an ensemble of conformations. The first approach is to calculate the ensemble-averaged mean-square angle $\langle\Theta^2\rangle$, dependent on segment length s[21]:

$$\langle\Theta^2(s)\rangle_{2D} = \frac{C}{L_p} \quad (4)$$

The second approach is to compute L_p from the ensemble-averaged mean-square end-to-end distances $\langle E^2\rangle$ of the fibrils[21]:

$$\langle E^2(s)\rangle_{2D} = 4L_pC\left(1 - \frac{2L_p}{C}\left(1 - e^{-C/2L_p}\right)\right) \quad (5)$$

If the fibrils are not equilibrated, the conformation depends on the surface adsorption mechanism and the model described above only yields an apparent persistence length.[21]

Table 7.1: Conformational statistics of HEWL amyloids adsorbed on either mica or glass and imaged by AFM under different conditions (dried or in liquid). The persistence lengths were computed taking into account only fibrils longer than 2 µm.

Sample	$\langle C\rangle$(µm)	$L_{p\langle\Theta^2\rangle}$ (µm)	$L_{p\langle E^2\rangle}$ (µm)	# of fibrils
Mica dried	4.1 ± 2.0	4.4	6.1	99
Mica liquid	3.2 ± 1.3	2.5	3.1	43
Glass dried	3.4 ± 1.3	3.8	4.6	70

We followed both approaches to analyze L_p based on AFM images of the HEWL amyloid fibrils imaged on mica. For all samples, only fibrils with a length over 2 µm were used in the analysis to ensure that the transverse undulations of the fibrils are resolvable in AFM images. The mean-square angle $\langle\Theta^2\rangle$ of dried fibrils was plotted as a function of contour length C and fitted with equation (4) (Figure 7.2a). We found an average value of L_p of 4.8 µm for a dataset of 99 fibrils (Table 7.1). However, the linear fit is quite poor, indicating that the mica surface influences the equilibration of the fibrils[21]. A better linear fit was obtained when the offset was a free parameter (grey line in Figure 7.2a), as has been proposed before[21], although this fit is not in accordance to equation (4). This fit results in L_p = 4.4 µm, slightly lower than the value of 4.8 µm obtained with

the fit using equation (4). To investigate whether drying affects the apparent persistence length, we also analyzed the shapes of hydrated fibrils imaged on mica using liquid AFM. Based on measurements on 43 fibrils, the average persistence length was L_p = 2.5 µm for a linear fit with zero offset and L_p = 2.4 µm for a linear fit with non-zero offset. Thus, the hydrated fibrils appear two-fold more flexible than the dried fibrils. It is difficult to conclude whether this difference corresponds to a real change in fibril stiffness. As explained above, the different sample preparation protocols for liquid AFM and air-AFM may select for a different fibril population on the surface. In support of this explanation, the population of dried fibrils that was used for persistence length measurements was on average longer than that of the hydrated fibrils, with average contour lengths of respectively 4.1 ± 2.0 µm and 3.2 ± 1.3 µm. Moreover, the differences in sample preparation may also affect the binding and equilibration of fibrils on the surface. To resolve this issue, it will be interesting in future work to perform AFM-based nanoindentation to measure the Young's modulus independent of fibril conformation as has been shown before for α-synuclein amyloid fibrils[34].

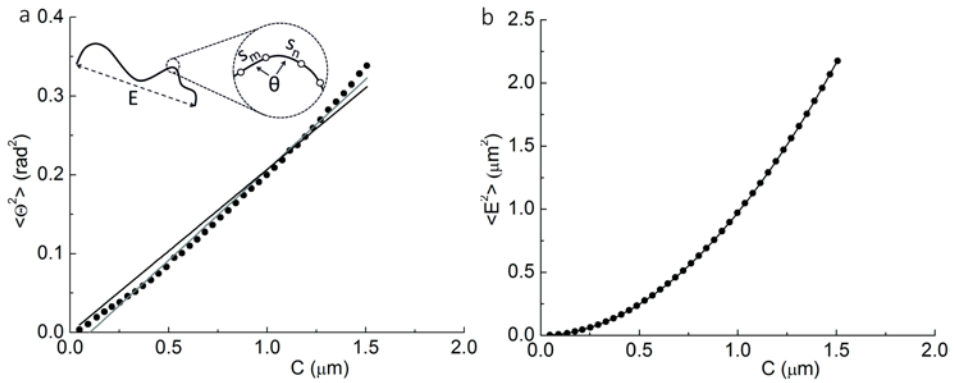

Figure 7.2: a) $\langle \Theta^2 \rangle$ as a function of contour length C of dried fibrils imaged on mica. The dataset was fitted with equation (4) (black line). Grey line is the linear fit where the offset is a free parameter. Inset shows a fibril with end-to-end length E and angle Θ between segments s_m and s_n. b) Mean-square end-to-end distance $\langle E^2 \rangle$ plotted as a function of contour length C. Black line is the fit with equation (5).

To investigate whether the surface affects the conformation of the fibrils, we compared the results obtained for fibrils adsorbed on mica with similar experiments on glass. Previous experiments with intermediate filaments showed that these filaments appeared more flexible on mica than on glass, because mica traps the fibrils on the surface before they are thermally equilibrated.[21] In total, 70 dried fibrils with an average length of C = 3.4 ± 1.3 µm were analyzed. The fit for the plot of $\langle \Theta^2 \rangle$ as a function of C using equation (4) gave an offset close to zero. For a forced-fit through zero, we found

L_p = 3.8 μm, while for a fit in which the intercept was a free parameter, L_p = 3.6 μm. This value of L_p lies in between the values measured for fibrils imaged in liquid and in air on mica. We conclude that the conformation of the amyloid fibrils imaged on mica may be affected by trapping on the surface. Therefore, to obtain a more precise measure of the persistence length from conformations measured on mica, fibril-surface interactions should be incorporated into the statistical model.

To test the sensitivity of the persistence length values on the analysis method, we also analyzed L_p for the same datasets using equation (5). The squared end-to-end length E^2 was plotted as a function of C and fitted with equation (5), as shown in Figure 7.2b for dried fibrils imaged on mica. We found L_p = 6.1 μm for dried fibrils imaged on mica and L_p = 3.1 μm for hydrated fibrils imaged in liquid on mica (Table 7.1). For dried fibrils imaged on glass, we determined L_p = 4.6 μm. For all samples the apparent L_p is larger when determined using equation (5) instead of equation (4). We anticipate that, because L_p is larger than the contour length of most of the fibrils, the analysis method based on equation (5) is less sensitive than the method based on equation (4) because it only takes into account the first bending mode. In contrast, equation (4) determines the bending of short segments of the fibril, resulting in a better estimation of L_p.

Because the confinement of the fibrils on a surface and drying can influence their apparent persistence length, we also determined the mechanical properties of fibrils freely fluctuating in liquid. The fibrils were fluorescently labeled and confined within a thin, quasi-two-dimensional layer between two non-sticky glass surfaces to ensure that the fibrils remained in focus. The sample chamber was well-sealed to prevent evaporation and fluid flows, so that only thermal forces acted upon the fibrils. Figure 7.3 shows 9 frames of a movie of a single fibril that exhibits thermal bending fluctuations. We imaged fluctuating single fibrils with lengths ranging between approximately 3 and 20 μm. Most fibrils showed only minor bending fluctuations, similar to the fibril shown in Figure 7.3.

We analyzed the images of the fibrils using statistical analysis of the time-dependent ensemble of shapes that a single fibril adopts when subjected to thermal forces[31]. The fluorescence images were analyzed based on a fibril contour representation expressed in a spectral basis of orthogonal polynomials, developed by Valdman et al.[27,28] For each image, the contour was fitted and the first 8 modes were analyzed. In Figure 7.4a, an example of the mode variances of the fluctuations of a fibril with a contour length of 3.9 μm is shown. The dashed line represents a fit to the worm-like chain model[31]. For this fibril, we analyzed 111 frames and determined L_p = 0.8 μm.

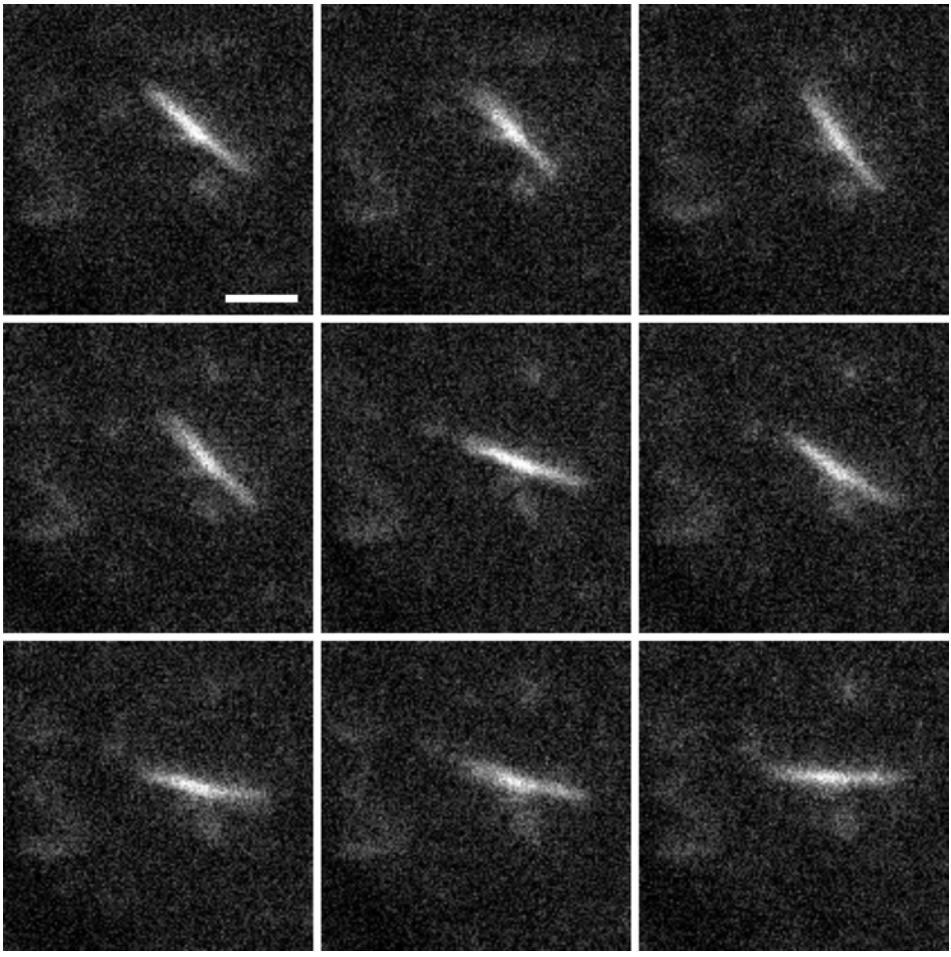

Figure 7.3: Fluorescence images of a single HEWL amyloid fibril labeled with Nile Red. Images were recorded at 4.9 fps with an exposure time of 100 ms. Time between subsequent images shown here is 0.2 s. The fibril is free to perform rotational and translational diffusion, indicating that the top and bottom glass surfaces are well passivated. Bending fluctuations are barely perceptible. Scale bar is 2 µm.

We applied this method to a total of 8 single amyloid fibrils with contour lengths between 3.4 µm and 4.7 µm. Per fibril, 46 to 280 images were analyzed to determine L_p. We obtained a range of persistence lengths between 0.7 µm and 6.7 µm (Figure 7.5 and Table 7.2). The average value of L_p for this small dataset of 8 fibrils was 2.4 µm, while the average contour length C was 3.9 ± 0.5 µm. For this analysis, two independent sources of error have to be considered. Noise in the microscopy images causes a localization error when localizing the filament contour.

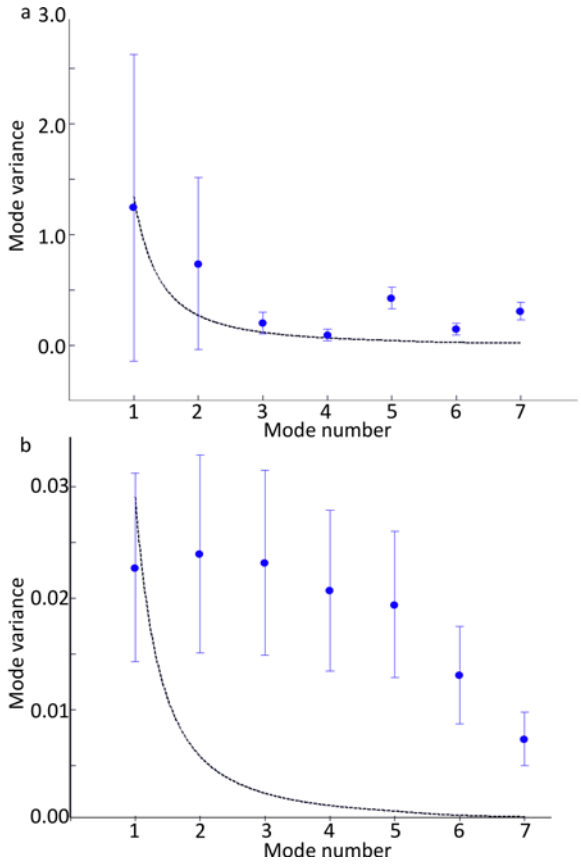

Figure 7.4: Mode variance (nondimensional) plotted as a function of mode number for the thermal fluctuations of a fibril. Dashed lines are the fits with a worm-like chain model. a) Results for a fibril with a contour length 3.9 µm and a persistence length of 0.8 µm. b) Results for a fibril with a contour length 9 µm whose bending fluctuations are too small to analyze by video tracking.

Table 7.2: Overview of the contour length, persistence length determined based on thermal fluctuations in free solution, and number of frames that was analyzed per fibril.

Fibril	C (µm)	L_p (µm)	# of images
1	3.4	0.7	97
2	3.5	1.6	325
3	3.6	1.7	46
4	3.7	2.1	238
5	3.9	0.8	111
6	4.0	1.4	104
7	4.6	6.7	129
8	4.7	4.5	280

The second source of error, the sampling error, is caused by the finite number of images which is analyzed per fibril. It was calculated that a good approximation of L_p is obtained when 100 or more images per fibril are analyzed.[27] We analyzed for 7 out of 8 fibrils more than 100 images (Table 7.2). For simulated images of a fibril with known L_p and a high noise level, a measurement uncertainty of approximately 10% for L_p has been predicted.[27] This indicates that the range of L_p that we observed for the amyloid fibrils is due to structural heterogeneity of the fibrils and not to errors in the analysis.

We also obtained time-lapse movies of two long fibrils showing no visible fluctuations. In these cases, it was impossible to determine the persistence length (Figure 7.4b). The fact that we did not observe fluctuations even though the fibrils had long lengths of 9 and 19 μm indicates that their persistence length was larger than this length scale.

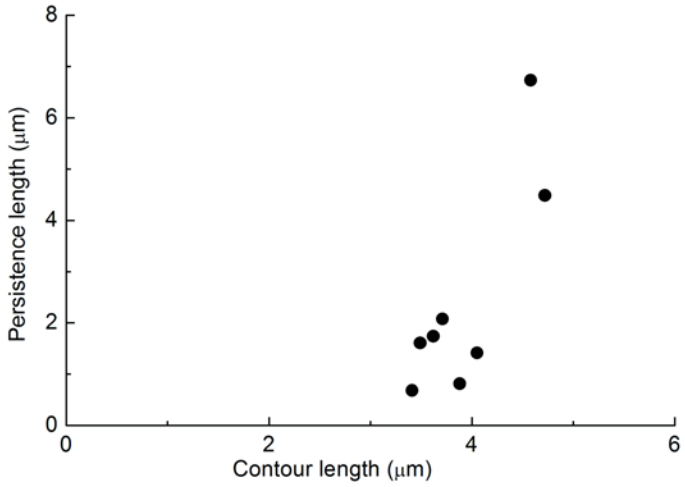

Figure 7.5: Persistence length plotted as a function of contour length for 8 individual fibrils, determined based on their spectrum of thermal fluctuations.

The average value of L_p that we obtained from time-lapse imaging of single fibrils in solution is similar to that of hydrated fibrils adsorbed on mica and slightly lower than the values measured for dried fibrils on glass. However, the dataset of the fluctuating fibrils is small (8 fibrils), so this comparison is only qualitative until we have more data. Nevertheless, we can already conclude that there is a pronounced variability in persistence length among fibrils, which probably drives the broad distribution that is also seen in AFM. This variability is not surprising given the polymorphism of the amyloid fibrils that we observe in our AFM images. For a homogeneously elastic cylindrical rod of radius r, L_p varies as r^4, indicating that polydispersity in diameter will result in a large spread of L_p. Unfortunately it is not possible to determine the diameter

of the analyzed fibrils from our fluorescent microscopy images, so we cannot conclude whether the large range of persistence lengths is related only to a variation in fibril diameter or whether the molecular packing structure of the fibrils varies too. Furthermore, we do not know the shape of the fibril cross-section. For amyloid fibrils composed of 2 or more protofilaments, ribbon-like as well as nanotube-like packings have been reported.[18,35,36] Another complicating factor is that the stiffness of fibrils comprised of multiple protofilaments may be influenced by sliding between protofilaments.[37]

It has been reported previously that L_p of amyloids fibrils formed upon incubation of HEWL for several days at pH=2.0 and T=60°C is approximately 2.5 μm.[38] This analysis was based on AFM images of dried fibrils on mica or graphite, though no differences between the surfaces were specified. Also for amyloid fibrils formed from other proteins, like β-lactoglobulin and ovalbumin, persistence lengths between 1 and 3 μm have been reported.[16,18,38,39]

Conclusions

We determined the persistence length L_p of amyloid fibrils formed from HEWL using two approaches: by analysis of the time-dependent thermal fluctuations of individual fibrils in an aqueous environment, and by the analysis of the shapes of an ensemble of fibrils adsorbed on a surface. With both methods, we obtained persistence lengths of a few micrometers. The analysis of surface-adsorbed fibrils imaged with AFM showed that interactions of the fibrils with the substrate influenced the measurements of L_p: dried fibrils on mica had a larger apparent L_p than dried fibrils on glass. Hydrated fibrils imaged on mica had a smaller apparent L_p than dried fibrils on mica, but this difference may be a consequence of differences in sample preparation, leading to the analysis of a different population of fibrils. The analysis of the time-dependent thermal fluctuations of individual fibrils revealed a broad variability in L_p-values over almost an order of magnitude, with L_p ranging from 0.7 up to at least 6.7 μm. This variability indicates a large heterogeneity between fibrils in terms of diameter and/or internal packing structure. In future, we will enlarge this dataset to obtain a more precise overview of the persistence length of HEWL amyloid fibrils.

Materials and methods

HEWL fibril formation. Hen egg white lysozyme powder (HEWL, Sigma Aldrich cat # 62970) was dissolved in a HCl solution (pH=2.0) and the pH was immediately adjusted to pH=2.0. HEWL was dissolved by stirring the solution for 1 hr at 4°C. To remove traces of electrolytes, the solution was dialyzed against a HCl solution (pH=2.0) at 4°C using a slide-a-lyzer (Thermo Scientific cat. #87732) with a molecular weight cut-off (MWCO) of

10 kDa. Aggregates were removed by filtration with a 0.1 µm filter (Sigma Aldrich #F7523). The protein concentration was calculated based on measurements of light absorption at 280 nm with a Nanodrop spectrophotometer (Thermo Scientific), using an extinction coefficient of 37,752 $M^{-1}cm^{-1}$.[40] Amyloid fibrils were formed by incubation of 30 mL of the monomer solution at a concentration of 1 mM in a polypropylene tube in an oven at 65°C for 7 days, while the solution was stirred using a magnetic stirrer. After 7 days, samples were quenched on ice water and fibrils were separated from small aggregates and monomers by filtration using centrifugal filters (Amicon, Millipore cat.#UFC910024) with a MWCO of 100 kDa. Prewashed filters were centrifuged at 1000 *g* for 30 min and samples were subsequently washed 3 times with a HCl solution (pH=2.0) by repeating the centrifugation.

Glass surface passivation. Microscope glass slides and cover slips (Menzel Glaser, Thermo Fisher Scientific) were cleaned by incubation in base piranha (H_2O: NH_4:H_2O_2 in a volume ratio of 7:1:1) for 12 min. Glass slides and cover slips were subsequently washed with MilliQ water, dried with nitrogen and incubated for 1 hr in 2.5% 3-mercapto propyl trimethoxy silane (3-MPTS) in toluene. Silanized glass was washed first with toluene and then with ethanol, dried with nitrogen and baked overnight in an oven at 100°C. PEG (20 kDa mPEG maleimide, Laysan Bio Inc.) was melted on the glass and incubated in an oven at 80°C. After 1.5 to 2.0 hrs, PEG was washed off using preheated ethanol at a temperature of approximately 60°C and the glass was dried with nitrogen. Slides were used for experiments the same day. We also tried to bind mPEG to silanized glass by incubation with mPEG dissolved in water or phosphate buffer at room temperature, but this did not result in sufficient surface coverage to prevent nonspecific adhesion of fibrils to the surface.

Labeling and fluorescence microscopy. Nile Red (Sigma Aldrich cat. #72485) was dissolved in ethanol at a concentration of 10 µM and filtered using a 0.1 µm syringe filter to remove aggregates. HEWL amyloid fibrils at a concentration of 10 µM were mixed in a 1:1 ratio with the Nile Red solution, and further diluted in HCl solution (pH=2.0) in a 1:50 ratio. A drop of 1 µL was sandwiched between the glass slide and the cover slip and gentle pressure was applied to spread the solution. The chamber was sealed with Valap (Vaseline, lanolin and paraffin in a 1:1:1 ratio). Samples were imaged using an epi-fluorescence wide field microscope (Ti-Eclipse Nikon) equipped with a 100x oil immersion objective (numerical aperture 1.4) and a digital CCD camera (Coolsnap HQ2 Photometrics, Tucson AZ). Images were taken at 4.9 frames per second with an exposure time of 100 ms. Typically up to 400 frames could be collected before the sample photobleached after approximately 80 s.

Data analysis. Wide field epifluorescence time-lapse images of individual fluctuating amyloid fibrils were analyzed using analysis software in Matlab developed by P. Atzberger et al.[27,28] The analysis is based on the global fitting of an entire trial contour at once to a fluorescent image. To determine the initial contour of the fibril, a box that encloses the brightest pixels in the image is drawn. The diagonal that connects the corners with the highest average intensity is the initial contour for fitting. The contour representation is expressed in terms of the tangent angles parameterized by the arc-length and expanded in a basis of orthogonal polynomials. The flexural rigidity of the fibril was inferred by statistical analysis of the ensemble of biopolymer configurations at thermal equilibrium. By analysis of simulated ensembles of fluorescent images of a simulated fiber with known L_p and varying levels of background noise and gap artifacts (irregularities in fluorophore labeling), an error of <10% on the estimated persistence length was observed for the highest background noise. For a majority of low-to-moderate noise cases, the error was < 1%.

Atomic Force Microscopy. Filtered fibril suspensions were diluted to protein concentrations of approximately 0.01% (w/w) and 15 µL of the suspension was incubated on freshly cleaved mica (Muscovite mica V-4, Electron Microscopy Sciences) or glass slides that were rinsed with iso-propanol and dried by nitrogen. After 3 minutes, the surface of the mica or glass slide was washed with HCl solution at pH=2.0, and dried in air. Atomic force microscopy imaging was performed on a Dimension 3100 Scanning Probe Microscope (Bruker) using silicon cantilevers (TESPA, force constant 42 N/m, Bruker). For liquid AFM, the filtered fibril suspensions were diluted to protein concentrations of approximately 0.1% (w/w). A drop of the fibril suspension was pipetted on freshly cleaved mica, and measurements were started immediately at room temperature using silicon nitride cantilevers (SNL-10, force constant 0.24-0.35 N/m, Bruker). All images were flattened using Nanoscope 6.14 software.

Acknowledgment

We thank Norbert Mücke for providing software for persistence length analysis. This work is part of the Industrial Partnership Programme (IPP) Bio(-Related) Materials (BRM) of the Stichting voor Fundamenteel Onderzoek der Materie (FOM), which is financially supported by the Nederlandse Organisatie voor Wetenschappelijk Onderzoek (NWO). The IPP BRM is co-financed by the Top Institute Food and Nutrition and the Dutch Polymer Institute.

References

(1) Dobson, C. M. *Nature* **2003**, *426*, 884.
(2) Knowles, T. P.; Vendruscolo, M.; Dobson, C. M. *Nature reviews. Molecular cell biology* **2014**, *15*, 384.
(3) Jayasinghe, S. A.; Langen, R. *Biochimica et Biophysica Acta (BBA) - Biomembranes* **2007**, *1768*, 2002.
(4) Engel, M. F. M. *Chemistry and Physics of Lipids* **2009**, *160*, 1.
(5) Milanesi, L.; Sheynis, T.; Xue, W.-F.; Orlova, E. V.; Hellewell, A. L.; Jelinek, R.; Hewitt, E. W.; Radford, S. E.; Saibil, H. R. *Proceedings of the National Academy of Sciences* **2012**, *109*, 20455.
(6) Smith, J. F.; Knowles, T. P. J.; Dobson, C. M.; MacPhee, C. E.; Welland, M. E. *Proceedings of the National Academy of Sciences U.S.A.* **2006**, *103*, 15806.
(7) Knowles, T. P.; Fitzpatrick, A. W.; Meehan, S.; Mott, H. R.; Vendruscolo, M.; Dobson, C. M.; Welland, M. E. *Science* **2007**, *318*, 1900.
(8) Otzen, D.; Nielsen, P. H. *Cellular and Molecular Life Sciences* **2008**, *65*, 910.
(9) Fowler, D. M.; Koulov, A. V.; Balch, W. E.; Kelly, J. W. *Trends in biochemical sciences* **2007**, *32*, 217.
(10) van der Linden, E.; Venema, P. *Current Opinion in Colloid & Interface Science* **2007**, *12*, 158.
(11) Reynolds, N. P.; Styan, K. E.; Easton, C. D.; Li, Y. L.; Waddington, L.; Lara, C.; Forsythe, J. S.; Mezzenga, R.; Hartley, P. G.; Muir, B. W. *Biomacromolecules* **2013**, *14*, 2305.
(12) Li, C. X.; Mezzenga, R. *Nanoscale* **2013**, *5*, 6207.
(13) Ryan, D. M.; Nilsson, B. L. *Polymer Chemistry* **2012**, *3*, 18.
(14) Knowles, T. P. J.; Buehler, M. J. *Nature Nanotechnology* **2011**, *6*, 469.
(15) Scheibel, T.; Parthasarathy, R.; Sawicki, G.; Lin, X. M.; Jaeger, H.; Lindquist, S. L. *Proceedings of the National Academy of Sciences of the U.S.A.* **2003**, *100*, 4527.
(16) vandenAkker, C. C.; Engel, M. F. M.; Velikov, K. P.; Bonn, M.; Koenderink, G. H. *Journal of the American Chemical Society* **2011**, *133*, 18030.
(17) Relini, A.; Torrassa, S.; Ferrando, R.; Rolandi, R.; Campioni, S.; Chiti, F.; Gliozzi, A. *Biophysical Journal* **2010**, *98*, 1277.
(18) Adamcik, J.; Jung, J. M.; Flakowski, J.; De Los Rios, P.; Dietler, G.; Mezzenga, R. *Nature Nanotechnology* **2010**, *5*, 423.
(19) Gosal, W. S.; Morten, I. J.; Hewitt, E. W.; Smith, D. A.; Thomson, N. H.; Radford, S. E. *Journal of Molecular Biology* **2005**, *351*, 850.
(20) Mucke, N.; Klenin, K.; Kirmse, R.; Bussiek, M.; Herrmann, H.; Hafner, M.; Langowski, J. *Plos One* **2009**, *4*.
(21) Mücke, N.; Kreplak, L.; Kirmse, R.; Wedig, T.; Herrmann, H.; Aebi, U.; Langowski, J. *Journal of Molecular Biology* **2004**, *335*, 1241.
(22) Volpatti, L. R.; Vendruscolo, M.; Dobson, C. M.; Knowles, T. P. J. *ACS Nano* **2013**, *7*, 10443.
(23) Aymard, P.; Nicolai, T.; Durand, D.; Clark, A. *Macromolecules* **1999**, *32*, 2542.
(24) Sagis, L. M. C.; Veerman, C.; van der Linden, E. *Langmuir* **2004**, *20*, 924.
(25) Knowles, T. P. J.; Buehler, M. J. *Nature Nano* **2011**, *6*, 469.
(26) Castro, Carlos E.; Dong, J.; Boyce, Mary C.; Lindquist, S.; Lang, Matthew J. *Biophysical Journal* **2011**, *101*, 439.
(27) Valdman, D.; Atzberger, Paul J.; Yu, D.; Kuei, S.; Valentine, Megan T. *Biophysical Journal* **2012**, *102*, 1144.
(28) Valdman, D.; Lopez, B. J.; Valentine, M. T.; Atzberger, P. J. *Soft Matter* **2013**, *9*, 772.

(29) Brangwynne, C. P.; Koenderink, G. H.; Barry, E.; Dogic, Z.; MacKintosh, F. C.; Weitz, D. A. *Biophysical Journal* **2007**, *93*, 346.
(30) Brangwynne, C. P.; Koenderink, G. H.; MacKintosh, F. C.; Weitz, D. A. *Physical Review Letters* **2008**, *100*, 118104.
(31) Gittes, F.; Mickey, B.; Nettleton, J.; Howard, J. *Journal of Cell Biology* **1993**, *120*, 923.
(32) Duggal, R.; Pasquali, M. *Physical Review Letters* **2006**, *96*.
(33) Schiffels, D.; Liedl, T.; Fygenson, D. K. *ACS Nano* **2013**, *7*, 6700.
(34) Sweers, K.; van der Werf, K.; Bennink, M.; Subramaniam, V. *Nanoscale Research Letters* **2011**, *6*.
(35) Lara, C. c.; Adamcik, J.; Jordens, S.; Mezzenga, R. *Biomacromolecules* **2011**, *12*, 1868.
(36) Adamcik, J.; Lara, C.; Usov, I.; Jeong, J. S.; Ruggeri, F. S.; Dietler, G.; Lashuel, H. A.; Hamley, I. W.; Mezzenga, R. *Nanoscale* **2012**, *4*, 4426.
(37) Bathe, M.; Heussinger, C.; Claessens, M.; Bausch, A. R.; Frey, E. *Biophysical journal* **2008**, *94*, 2955.
(38) Lara, C.; Usov, I.; Adamcik, J.; Mezzenga, R. *Physical Review Letters* **2011**, *107*, 238101.
(39) Jordens, S.; Adamcik, J.; Amar-Yuli, I.; Mezzenga, R. *Biomacromolecules* **2010**, *12*, 187.
(40) Mishra, R.; Sorgjerd, K.; Nystrom, S.; Nordigarden, A.; Yu, Y. C.; Hammarstrom, P. *Journal of Molecular Biology* **2007**, *366*, 1029.